PERGAMON

Deep-Sea Research II 49 (2002) 4097–4113

DEEP-SEA RESEARCH
PART II

www.elsevier.com/locate/dsr2

The boiling-water phenomena at Camarinal Sill, the strait of Gibraltar

Miguel Bruno[a,*], José Juan Alonso[a], Andrés Cózar[b], Juan Vidal[a], Antonio Ruiz-Cañavate[a], Fidel Echevarría[b], Javier Ruiz[b]

[a] *Departamento de Física Aplicada. Facultad de Ciencias del Mar. Universidad de Cádiz, 11510, Puerto Real Cádiz, Spain*
[b] *Area de Ecología, Facultad de Ciencias del Mar, Universidad de Cádiz, 11510, Puerto Real, Cádiz, Spain*

Received 3 May 2000; received in revised form 28 April 2001; accepted 18 July 2001

Abstract

A detailed description of high-amplitude steady topographic internal waves recorded at Camarinal Sill during a survey on the R.V. "*Investigador*" is presented. These internal waves are generated during the maximum outflow (westward) stage of the tidal current and remain over the sill for more than 4 h until the outflow slackens, then being released towards the Mediterranean. Their amplitudes are comparable to the well-known internal bore of Camarinal Sill, occurring during maximum outflow during spring tides. However, they respond to a different physical origin and their spatial features are also quite different. In fact, the favourable hydraulic conditions for the generation of steady waves over the sill inhibit the internal bore generation, and vice versa. Analysis of the observations suggests that steady internal waves are the result of a resonant response of the stratified fluid over the sill to the forcing of the flow on the across-sill topography. An important consequence of the steady internal waves with clear biological implications is the significant mixing phenomena that are induced. Mixing is enabled by an enhancement of the shear at the trough together with a significant induced vertical advection.

1. Introduction

The surface signatures associated with the interaction of flows with banks, internal waves, and frontal boundaries are well-known oceanographic phenomena (New and Pingree, 1992; Richez, 1994). Surface signatures associated with internal waves usually consist of slight modulations (surface slicks) of the surface-wave spectra. In the case of more energetic internal waves, signatures can consist of a chaotic sea of breaking short waves organised in rectangular plumes aligned with the internal-wave crests (New and Pingree, 1992).

The Strait of Gibraltar is one place where intense internal waves events occur and therefore intense surface signatures are frequently observed. There are several papers on tracking the evolution of the surface signature by synthetic aperture radar, shore-based radar or on-board radar in order to study the propagation characteristics of the internal waves in the Strait of Gibraltar (Frasseto, 1964; Ziegenbein, 1969; Cavanie, 1972; La Violette et al., 1986; Richez, 1994; Watson and Robinson, 1990; Brandt et al., 1996).

Those surface signatures in the Gibraltar Strait are known by the local Spanish fishermen and

*Corresponding author.

0967-0645/02/$ - see front matter
PII: S0967-0645(02)00144-3

sailors as "hervideros" (boiling waters) and "hileros de corriente" (streamers), in reference to the visible behaviour of the surface waters (Ruiz-Cañavate and Rico, 1996). They were reported in the literature, for the first time, in the Spanish Navy Sailing Directions by Tofiño (1832), being mentioned and documented as well in the English Sailing Directory by Purdy (1840) and later editions of the Spanish Sailing Directions. A free translation of part of their description is as follows: "They appear instantaneously without previous signs. Suddenly a roughness in the sea surface appears as when the water is boiling, and a surfing chaotic sea is established. If wind and wind-induced forces are considered, the streamers are dangerous not only for smaller ships but for bigger ships also. Sometimes the vessel acquires a vortex motion without steerage". Hereafter we will refer to these surface signatures as boiling-water plumes (BWP).

Until now, most of the studies on internal waves in the Strait of Gibraltar have been focussed either on the internal tide (Boyce, 1975; Bray et al., 1990; Bruno et al., 2000) or the generation, release, and propagation of the internal bore that originates downstream of Camarinal Sill during maximum Mediterranean outflow (Armi and Farmer, 1988; Richez, 1994; Brandt et al., 1996; Izquierdo et al., 2001). Existing data about internal bores indicate that large-amplitude internal bores, travelling to the east, with amplitudes from crest to trough of more than 100 m, are generated downstream of the Camarinal Sill during spring tide when maximum outflow is established, being released at the early beginning of the tidal inflow. Those bores can have counterparts travelling westward in the form of small-amplitude internal bores released from east of Camarinal Sill at the end of tidal inflow.

However, there is a kind of internal wave that appears during the maximum Mediterranean outflow right on the Camarinal Sill, not on the lee side like the internal bore, staying there and establishing a steady-state situation for more than 4 h before being released towards the Mediterranean. Fig. 1 illustrates the intense boiling water plume associated with the crest of one of these steady trapped waves.

Fig. 1. Image of a boiling water plume at Camarinal Sill observed during a flood tide (flow toward west) around 14:00 GMT on November 24th 1998.

La Violette and Lacombe (1988) described an internal structure over the sill, which was formed in a maximum outflow phase of tidal current during a neap tide. That structure presented very similar behaviour as the observed in the present work, although they did not identify clearly what kind of wave it was. Richez (1994), using airbone synthetic aperture radar, found two different internal structures at Camarinal Sill. The first was obtained during a strong outflow phase of tidal current and corresponds to the internal bore with a clear surface signature located well downstream of Camarinal Sill. The second, performed during a weaker outflow, consisted of two lines following almost exactly the Camarinal Sill axis, and the first of them (from east to west) right on the eastern boundary of the sill. The latter structure is quite similar to that described in La Violette and Lacombe (1988).

From the aforesaid it is deduced that there are two kinds of large amplitude internal structures formed in the surrounding of Camarinal Sill during the flood phase of tidal current. The first one is the downstream internal bore, and a second one consists of a steady internal wave located right over the sill. Although in the existing literature the behaviour of the second structure have been described more or less precisely, their physical origin is unstudied and therefore is the subject of this paper.

Armi and Farmer (1988) found that the generation of internal bores is interrupted during neap

tides. However, our observations of trapped waves always were done in neap-tide periods. The common characteristic between the two phenomena is that they are established during the maximum outflow stage of the tide. On the basis of these first impressions, it seems that the occurrence of each phenomenon, internal bore and trapped-over-the-sill waves, is more probable during spring and neap tides, respectively.

The aim of the present work is twofold: (i) to define the physical origin of these waves and establish the differences, analogies and relationships with the internal bore, and (ii) to investigate the importance of the dynamics of water masses induced by this phenomenon so as to accentuate the mixing of particulate matter through the interface between the Atlantic and Mediterranean layers.

2. Experimental background

The survey that promoted our study was carried out through an agreement between the Applied Physics Department of the University of Cadiz and the Spanish Society for the fixed communication between Spanish and Morocco (SECEG). The University of Cadiz provided prognostic and real-time current data from a ship-mounted 150 KHz ADCP to assess the operations of sediment coring carried out by a drilling ship at Camarinal Sill. Taking advantage of the unlimited energy supply available for the ADCP, the recordings were taken at 1-min intervals, which provided a sufficiently high-temporal resolution to track with detail the changes in the velocity profiles induced by the passing of internal waves over the sill. The ADCP data were not only provided to tri-dimensional current velocity measurements, but they also provided echo intensity profiles that allowed detecting the reflector (suspended particulate matter) distributions, a useful way to visualise the stratification of the water column. The current measurements were extended from 20 to 250 m depth with a vertical resolution of 10 m.

Along with the ADCP measurements, some casts with a multi-parameter probe carrying CTD, transmissivity, dissolved oxygen, and pH sensors were performed when required. The vertical resolution of the CTD raw data was approximately of 1 cm. Subsequently they were filtered and subsampled to 1-m intervals.

The observations presented here were taken on the R.V. *Investigador* during November 1998. Unfortunately, since the operations could only be performed at low current velocities, the data acquisition always was made during neap tides, and thus our data will be only representative for these particular conditions.

The most remarkable internal wave feature we found in our survey was the high-amplitude internal waves trapped over Camarinal Sill. In order to study that feature, our methodology for measurements consisted of performing succesive sections of about 1 km at right angles to the main axis of Camarinal Sill, which is along the normal direction to the steady internal waves. The mean sampling interval in the horizontal along the sections was 22 m for the ADCP and 70 m for the multi-parameter probe. The zone of measurements was directly over the sill crest (Fig. 2).

3. Observations across the boiling water plumes

3.1. Physical properties

Most of the observational data presented here correspond to one of the most intense internal waves trapping observed during the survey. It was established about the 13:30 GMT on November 24, 1998, around the time of maximum flood tide (westward flow) during one of the most intense flood tides within the neap-tide cycle.

The surface signature of the waves consisted of three quasi-steady BWP, approximately 500 m wide and 4000 m long, aligned with the Camarinal Sill crest, the first of them (from east to west) right on the sill crest. Distance between crests was about 1 km. The most remarkable subsurface characteristic associated to these waves was the upwelling of their crests to within a few meters of the surface, producing an across-sill steady variation in the thickness of the stratified-flow layers. This feature is clearly illustrated by the salinity, temperature,

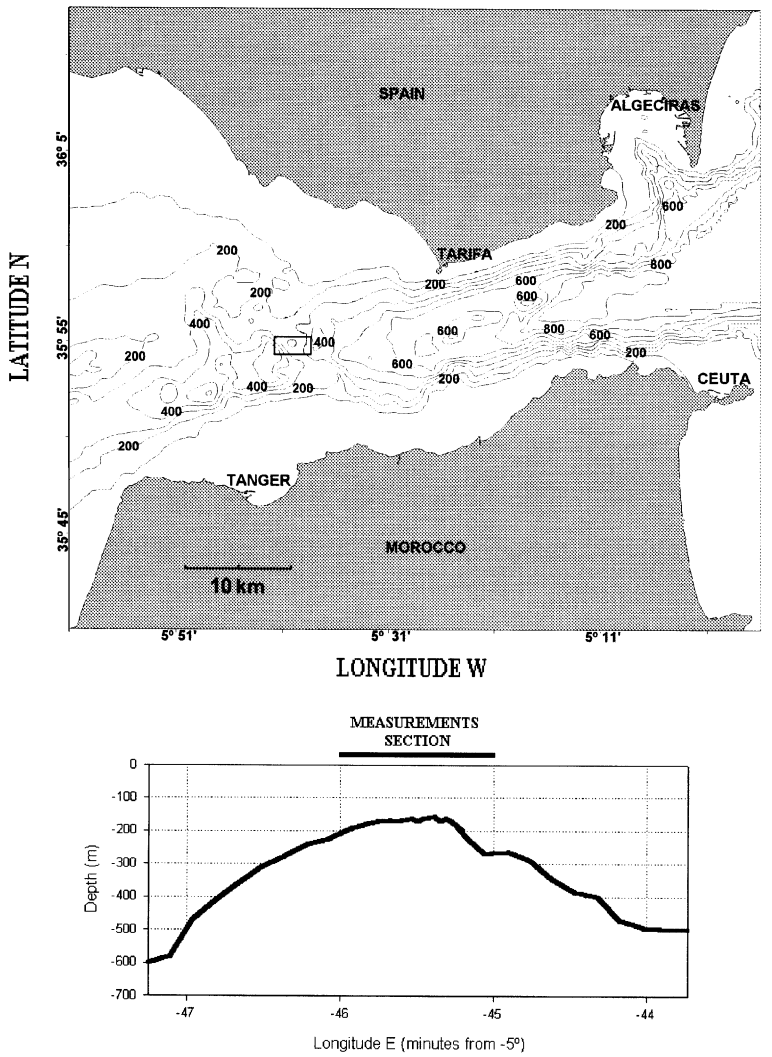

Fig. 2. Map of the Strait of Gibraltar with the location of the studied zone (isobaths are in meters). The lower figure represents a vertical section in the across-sill direction of Camarinal Sill bottom topography.

and density sections (Fig. 3). The variation in the thickness of the stratified layers conforms to a steady trapped wave with a wavelength of about 1000 m. The interface between Atlantic and Mediterranean layers (usually tracked by the 37.5 psu isohaline) rises up to 30 m depth in the crest of the wave and sinks nearly to 100 m depth in the trough. It must be noted that the amplitude of the waves is comparable to that associated with the internal bore.

The velocity field induced by the steady trapped waves is illustrated in Fig. 4. For comparison the velocity field immediately before the waves appearance is also presented. It should be noted that by this time the entire water column moved toward the Atlantic, showing, as expected, lower values in the upper layer. A strong horizontal velocity gradient in the transversal direction to the wave trains is created. In this way, the upper flow is accelerated in the crest and decelerated in the

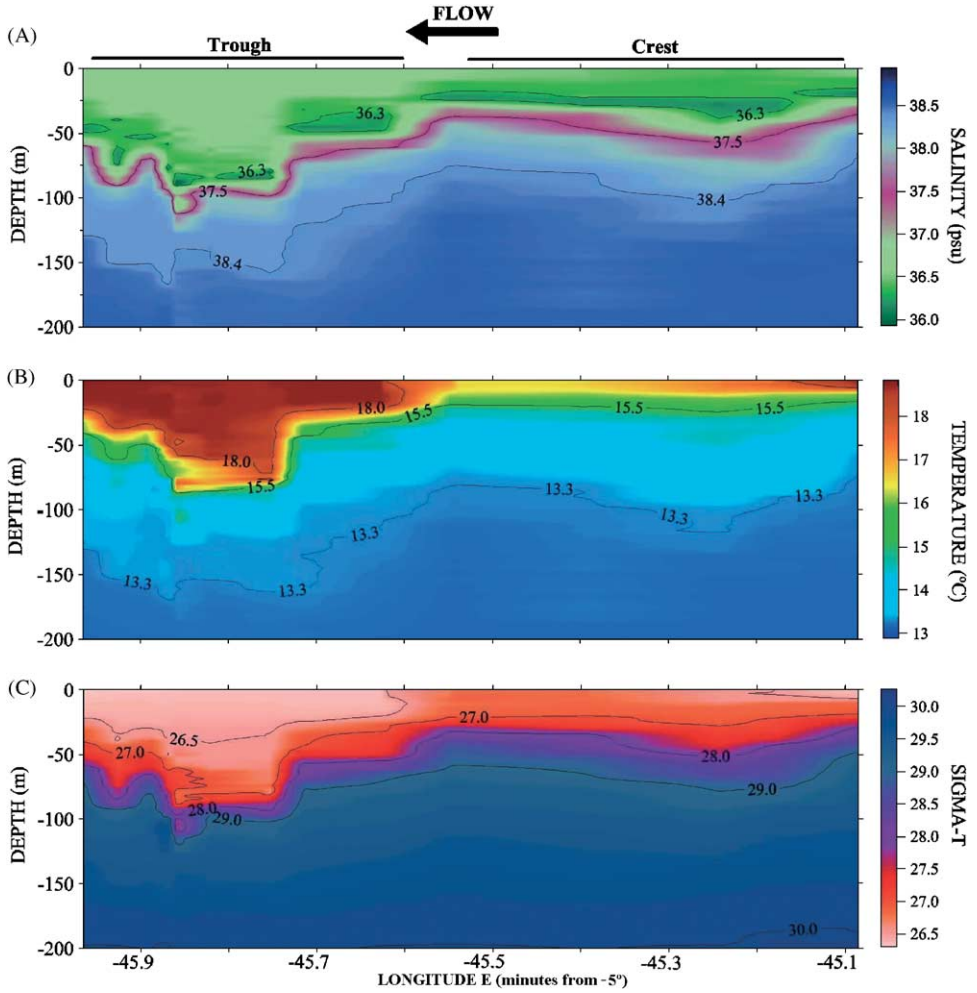

Fig. 3. Vertical sections of physical properties across the boiling water plumes observed during a flood tide (flow toward west) on November 24th 1998. (A) Salinity; (B) temperature; (C) density (σ_t).

trough. These abrupt changes in flow velocity around the wave crests are the responsible for the particularly intense chaotic breaking sea of the BWP at surface. In the lower layer a significant velocity gradient also is created, with velocities in the trough greater than those in the crest. The combined effect of the upper and lower layer velocity gradients is an enhancement of the vertical shear at the trough and its weakening at the crest. Significant vertical movements of the water are also induced. The vertical velocities are zero below the crest and trough, and the downward and upward velocities maxima go from crest to trough and from trough to crest, respectively (Fig. 5). This is in agreement with the stream lines deduced from the isopycnal distribution (Fig. 3).

The above-described features were maintained for more than 4 h until the flood tide slack and the ebb tide (eastward tidal flow) was nearly established. Then steady trapped waves were released towards the Mediterranean in similar fashion to a conventional internal bore.

It is interesting to focus our attention on the unique features that the time series of horizontal

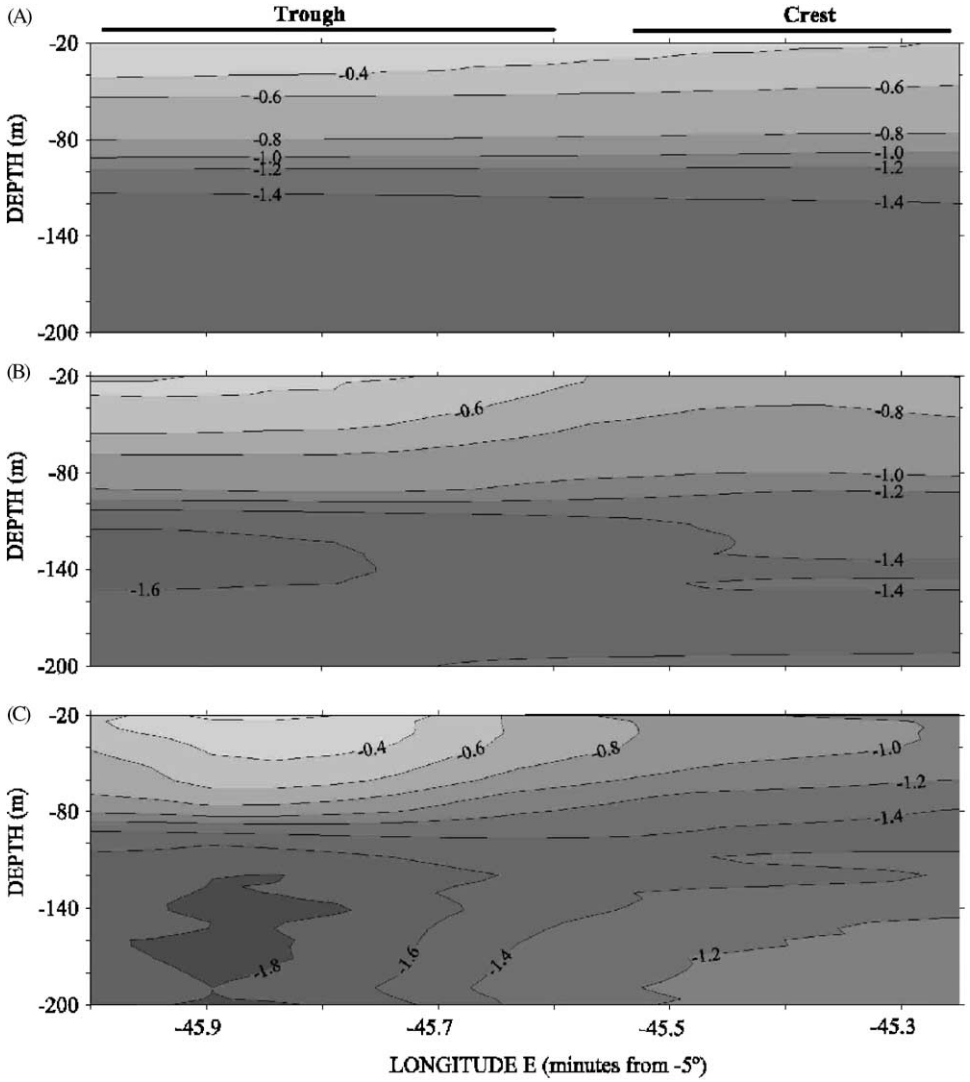

Fig. 4. Vertical sections of east–west horizontal velocity across the boiling water plumes observed during a flood tide (flow toward west) on November 24th 1998, velocities in m s^{-1}. (A) Situation prior to the waves establishement at 12:30 GMT; (B) in an early stage of the waves generation at 13:00 GMT; (C) one hour after the situation in (B).

velocity showed when the internal wave events were active. Since the vessel was performing repeated, forward and backward, traverses in the orthogonal direction to the wave trains, the ADCP recorded the variations of the velocity field induced by the arrested wave. The aspect of the time series of horizontal velocity when it is established can be seen in the Fig. 6. By this time the velocity records (say at 20 m depth) show high-amplitude oscillations due to the repetition of the transits across the arrested wave trains. In this way, these high-amplitude oscillations in the horizontal velocity during the outflow phase can be used as an indicator for arrested wave occurrence. From Fig. 6, it can be observed that during the time of our survey, there were four internal wave events, whose existence was verified by the visual observation of the

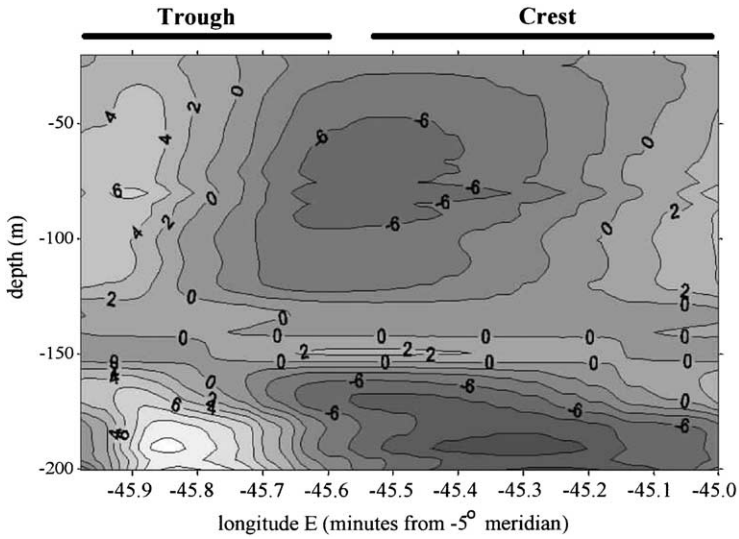

Fig. 5. Section of vertical velocity, expressed in cm s^{-1}, across the boiling water plumes for the same situation as in Fig. 4C. Positive (negative) values indicate upward (downward) direction.

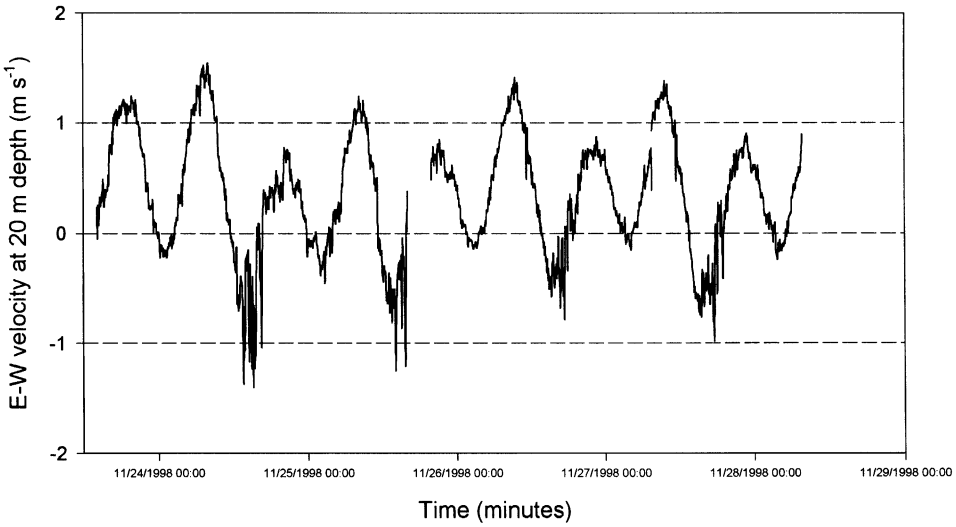

Fig. 6. Time series of the East–West velocity at 20 m depth, showing the singular high-amplitude oscillation associated to the arrested wave events.

persistent roughness at the sea surface. Although we recorded four events, we obtained a full data set (CTD plus ADCP) only during the first. For this reason, a complete analysis of the phenomenon was only possible for this event.

3.2. Associated mixing phenomena

An important consequence of the internal waves, with obvious biological implications, is the significant mixing that they induce. The mixing is enabled by an enhanced vertical shear created by

the waves at the trough along with the induced vertical advection. The enhancement of vertical shear at the trough can be observed in Figs. 7B and E, where two profiles of horizontal velocities, one at the crest and the another at the trough, are shown. Figs. 7C and F also show, at the same locations as the velocity profiles, the gradient Richardson number, $R_i = N^2/(\partial u/\partial z)^2$, where $N(z) = \sqrt{-(g/\rho_0)(\mathrm{d}\bar{\rho}/\mathrm{d}z)}$ is the squared buoyancy frequency; u is the east–west velocity; z the upward co-ordinate; ρ_0 is a reference density; and $\bar{\rho}(z)$ the undisturbed density profile. Values of $R_i < 0.25$ are presented in the trough profile at the top of the pycnocline, meaning that instabilities and mixing here are expected to occur. In fact, the fine structures in the salinity and temperature profile at the trough (Fig. 7D) indicate that mixing is taking place at the top of the pycnocline.

The induced vertical advection is the consequence of the slope of the streamlines following approximately the isopycnals. In this sense, it does not directly imply any transport across the pycnocline. However, it establishes a mean by which the suspended particulate matter close to the bottom is transported to shallower depths where turbulence may transport it to an upper layer. Therefore, an increasing of particulate matter concentration below the pycnocline is

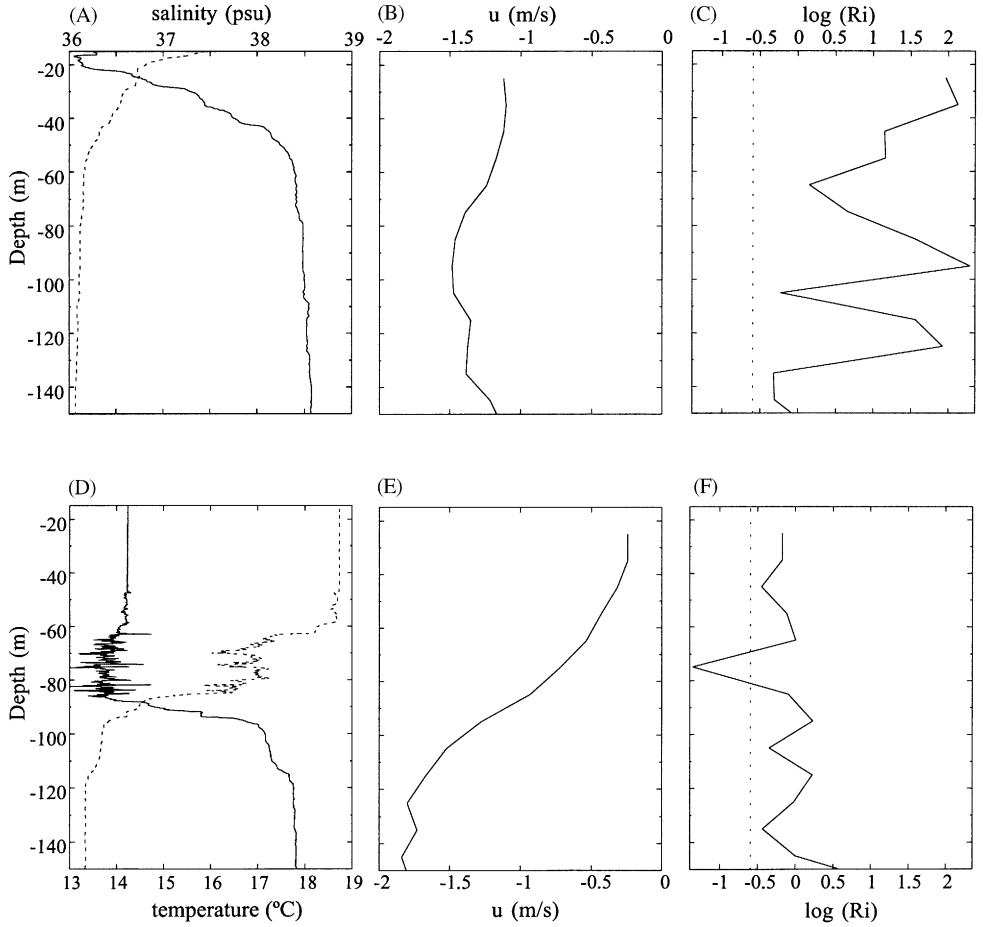

Fig. 7. Profiles of salinity, temperature, horizontal velocity and Richardson number logarithm. (A), (B) and (C) at the wave crest; (D), (E) and (F) at the trough. In (A) and (D) the dashed and solid lines are respectively for salinity and temperature. In (C) and (F) the vertical dashed lines indicate the value of $\log(Ri)$ corresponding to $Ri = 0.25$.

expected when the arrested waves are established. Evidence of this can be found in the Fig. 6 of Echevarría et al. (2002), corresponding to sections of turbidity, salinity, and vertical velocities across the wave trains. It can be observed that the transport of a particulate-rich lense (detected by higher turbidity zones) toward the upper layer and toward the bottom is clearly related with zones of upward (positive) and downward (negative) velocities, respectively.

Other evidence of the exchange of particulate matter in the lower layer linked to the arrested waves is shown in Fig. 8. At the end of this internal wave event, an increasing echo intensity (measured by ADCP) is observed in the lower layer. After maximum outflow, when the trapping was not observed, no increase in echo intensity was noted. While the waves are trapped, water masses of increased echo intensity were detected intermittently. Also, a general increase of echo intensity occurs after the beginning of tidal inflow and continues until the next outflow. The explanation for this observation could be (i) a further mixing induced by the release of arrested waves and their propagation toward the Mediterranean, (ii) an increased interfacial turbulence during the inflow, or (iii) a return of the suspended matter from the Tangier basin during the inflow. The second explanation does not seem adequate, since the velocity profiles showed a smaller shear than during the outflow. Therefore, there is no reason to think that during inflow a more intense turbulence existed between the Atlantic and Mediterranean layers than during the outflow. On the other hand, because the flow reversal in the lower layer did not take place during the inflow, the third explanation also seems unlikely. Thus the first one seems the most probable.

Vertical advection and mixing may combine to produce a suitable mechanism to carry the suspended nutrients from a lower layer to an upper one. Initially, vertical advection and mixing in the lower layer provide a general enrichment of particulate matter there. Then, the suspended particulate matter, which has arrived in the vicinity of the interface, may be injected into the upper layer by interfacial mixing. Finally, further mixing will occur after the waves are released during their subsequent propagation.

4. Physical origin of the steady arrested waves at Camarinal Sill

4.1. Hydraulic conditions over the sill before the waves appearance

Let us consider the two-layer approach with the internal Froude number

$$G^2 = \frac{U_1^2}{g'h_1} + \frac{U_2^2}{g'h_2}, \tag{1}$$

where U_i, ρ_i and h_i are the mean velocity, mean density and thickness for each layer ($i = 1, 2$ for upper and lower layer, respectively), $g' = g((\rho_2 - \rho_1)/\rho_2)$ is the reduced gravity, and g is gravity. The value of G^2 over the sill for the situation immediately before the generation is 0.73, with $U_1 = -0.74\,\mathrm{m\,s^{-1}}$, $\rho_1 = 1027.3\,\mathrm{kg\,m^{-3}}$, $h_1 = 90\,\mathrm{m}$, $U_2 = -1.46\,\mathrm{m\,s^{-1}}$, $\rho_2 = 1029.9\,\mathrm{kg\,m^{-3}}$ and $h_2 = 160\,\mathrm{m}$, indicating subcritical conditions here. The horizontal velocity field characterising this situation is shown in Fig. 4A.

Following with the two-layer approach, the dispersion relation for interfacial waves propagating over the sill, in the non-hydrostatic case, can be expressed as (Farmer and Armi, 1999):

$$c(k) = \frac{(U_1R_1 + U_2R_2)}{(R_1 + R_2)} \pm \frac{\sqrt{k^2(U_1R_1 + U_2R_2)^2 + (R_1 + R_2)(k^2U_1^2R_1 + k^2U_2^2R_2 - \rho_2 g'k)}}{k(R_1 + R_2)}, \tag{2}$$

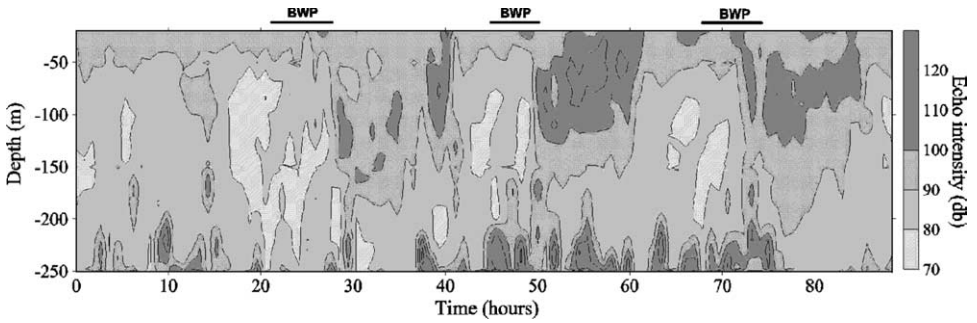

Fig. 8. Time evolution of the echo intensity (db) profiles taken by the ADCP over Camarinal Sill from 11/23–28/1998. The segments on the top indicate the time period during which the BWP were enabled.

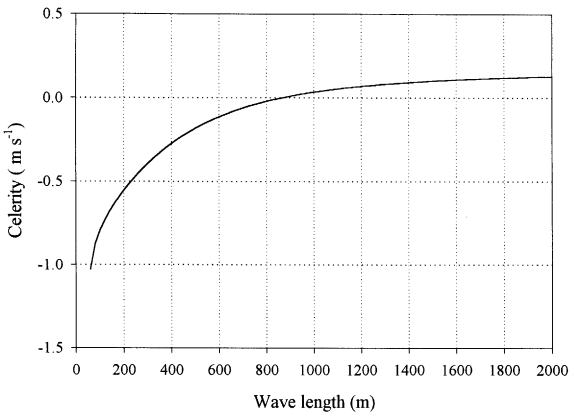

Fig. 9. Dispersion curve for interfacial waves under the hydraulic conditions prevailing over the sill prior to the trapped-wave appearance.

where c is the celerity of the wave with respect to a fixed frame, $R_i = \rho_i o \tanh(kh_i)$, $k = 2\pi/\lambda$ is the wave number, and λ is the wavelength.

Fig. 9 shows the dispersion relation for the conditions prior to the wave generation. Only waves with $\lambda > 800$ m show values of $c > 0$. Accordingly, only these waves may propagate over the sill against the flow. Also, internal waves with $\lambda \approx 800$ m may become trapped by the flow over the sill ($c = 0$). Recalling the results of Section 2, this value is close to the wavelength of the observed waves ($\lambda \approx 1000$ m). The next point to determine is the mechanism by which internal waves are generated.

A relevant element to explain the origin of the trapped waves is their relatively long steady-state period (more than 4 h), with amplitudes maintained even when the outflow is reduced significantly. This behaviour suggests that some type of resonant process is changed under the described hydraulic conditions, favouring wave amplification. In fact, a comparison between Figs. 4B and C shows that, initially (Fig. 4B), the disturbances of the velocity field are not as intense as prior to the waves appearance (Fig. 4A). One hour later (Fig. 4C), the disturbances of velocity are highly reinforced, which demonstrates that the waves evolve from a growth or resonant process. By the time of the situation presented in Fig. 4C, the waves have reached a steady-state where wave growth must be balanced by dissipation (Farmer and Armi, 1999). This steady-state is extended for 3 h more until the outflow is reduced enough for the waves trains to be released toward the Mediterranean.

Considering a wavelength of about 1 km, resonance may be related to the forcing of the flow over the across-sill topography, which must present a characteristic wavelength similar to the wavelength of the internal waves. In fact, a visual inspection of a representative across-sill topography (Fig. 10) shows that bottom irregularities have approximately 1000 m wavelength. This is a favourable resonant condition for the development of the observed waves. The resonance would act when their celerity tends to zero and it is accomplished, in accordance with Eq. (2), for interfacial waves propagating against the flow with $\lambda = 800$ m, which represents a value close to the wavelength of the bottom topography.

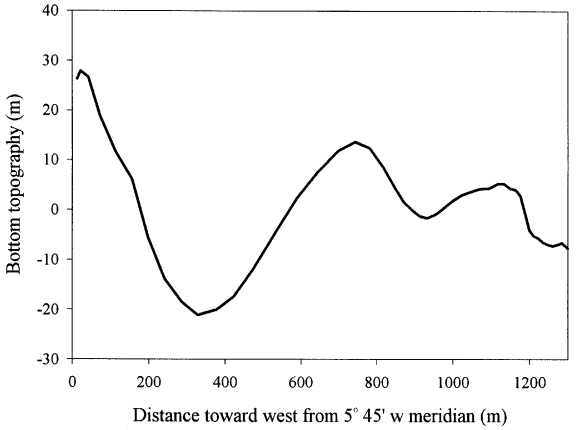

Fig. 10. Vertical section of the Camarinal Sill bottom topography in the across-sill direction. The values are respect to the mean value of the profile. Distances are from east to west.

In the frame of the two-layer approximation, we have proposed a generating mechanism that attempts to explain rather crudelty the observed phenomenon. A more realistic approach, however, may be to explore the possibility for the appearance of trapped waves taking into account continuous vertical profiles of density and velocity. This approach is considered in the next section.

4.2. Taylor–Goldstein equation and resonant wavelengths for steady topographic internal waves

The resonant wavelength of disturbances generated by topography in a continuously stratified fluid can be determined using the Taylor–Goldstein equation (Kundu, 1990), which consists of the hydrodynamic equations for the two dimensional non-rotating and non-hydrostatic case. Additional assumptions include an horizontally unbounded fluid, linear and Boussinesq approximations, negligible dissipative effects, flat bottom and horizontal homogeneity of the background stratification. In this case, the set of equations of motion, conservation of density and continuity that govern the perturbations read as:

$$\frac{\partial u}{\partial t}+U\frac{\partial u}{\partial x}+w\frac{\partial U}{\partial z}=-\frac{1}{\rho_0}\frac{\partial p}{\partial x}, \tag{3a}$$

$$\frac{\partial w}{\partial t}+U\frac{\partial w}{\partial x}=-g\frac{\rho}{\rho_0}-\frac{1}{\rho_0}\frac{\partial p}{\partial z}, \tag{3b}$$

$$\frac{\partial \rho}{\partial t}+U\frac{\partial \rho}{\partial x}-\frac{\rho_0 N^2 w}{g}=0, \tag{3c}$$

$$\frac{\partial u}{\partial x}+\frac{\partial w}{\partial z}=0, \tag{3d}$$

where u and w are the eastward and upward vertical component of the perturbation velocity in the cartesian co-ordinate system (x,z), $U(z)$ is the undisturbed background flow, p and ρ are the perturbations of pressure and density, ρ_0 is the mean sea water density, N is the buoyancy frequency and $\bar{\rho}(z)$ is the undisturbed density profile.

Defining a stream function through

$$u=\frac{\partial \psi}{\partial z}, \tag{4}$$

$$w=-\frac{\partial \psi}{\partial x} \tag{5}$$

and assuming normal mode solutions to the set of Eqs. (3)–(5) of the form:

$$(\rho,p,\psi)=[\hat{\rho}(z),\hat{p}(z),\hat{\psi}(z)]\mathrm{e}^{\mathrm{i}k(x-ct)}, \tag{6}$$

where c is the phase speed of the perturbation, we obtain the following equation for $\hat{\psi}$:

$$\frac{\mathrm{d}^2\hat{\psi}}{\mathrm{d}z^2}+\left[\frac{N^2}{(U-c)^2}-\frac{1}{(U-c)}\frac{\mathrm{d}^2U}{\mathrm{d}z^2}\right]\hat{\psi}=k^2\hat{\psi} \tag{7}$$

which along with the boundary conditions at the surface ($z=D$) and bottom ($z=0$),

$$\hat{\psi}(z=D)=0 \quad \hat{\psi}(z=0)=0 \tag{8}$$

constitute a Sturm–Liouville problem with eigenvalues k_n^2. The solution for a given c is a linear superposition of a set of eigenfunctions $\hat{\psi}_n(z)$, or vertical modes, satisfying the orthogonality condition

$$\int_0^D \hat{\psi}_n(z)\hat{\psi}_m(z)\,\mathrm{d}z=\delta_{nm}, \tag{9}$$

where δ_{nm} is the Kronecker delta.

For arbitrary $N(z)$ and $U(z)$ profiles, the problem (7) and (8) must be solved numerically. For steady disturbances, $c=0$, the solution of the eigenvalue problem determine if a steady internal

wave mode may be held under the background conditions specified by the $N(z)$ and $U(z)$ profiles. If such a mode exists, the corresponding eigenfunction defines the vertical distribution of each one of the disturbed flow variables. If the wavelength of the steady mode is close to the across-sill topographic wavelength, the conditions for resonance are met.

From Eq. (3c), after considering Eq. (3)–(5) and $c = 0$, we find that the amplitude of density perturbation for a given eigenfunction $\hat{\psi}_n(z)$ can be written as

$$\hat{\rho}_n(z) = -C\frac{\rho_0}{g}\frac{N^2}{U}\hat{\psi}_n, \tag{10}$$

where C is an arbitrary constant. The amplitude of velocity perturbations can be obtained from the set of equations,

$$\hat{u}_n(z) = C\frac{\partial\hat{\psi}_n}{\partial z}, \tag{11}$$

$$\hat{w}_n(z) = -\mathrm{i}Ck\hat{\psi}_n. \tag{12}$$

According to Eq. (6) the steady disturbances of density and velocities associated with the trapped resonant waves are then given by

$$\rho_n(x,z) = \hat{\rho}_n(z)\cos kx, \tag{13}$$

$$u_n(x,z) = \hat{u}_n(z)\cos kx, \tag{14}$$

$$w_n(x,z) = \mathrm{i}\hat{w}_n(z)\sin kx. \tag{15}$$

We have solved the eigenvalue problem (7) and (8) using the $N(z)$ and $U(z)$ profiles for the situation prior to the internal waves appearance (see horizontal velocities in Fig. 4A). Both profiles have been fitted to smoothed analytical functions (see Figs. 11A and B). We may now proceed to the numerical solution.

The results provide an eigenfunction with $\lambda = 1100$ m (Fig. 12A). Therefore, the associated oscillation mode has a wavelength very close to that of the topography (1000 m) and the conditions for such a mode becoming resonant are satisfied. The behaviour of the corresponding amplitudes of ρ, u and w with depth is also shown in Fig. 12. The value for C correspond to the maximum amplitude of the density perturbation allowed for a stable density profile. The maximum amplitude for all three variables corresponds to the maximum of $N(z)$ (Fig. 11C), and the amplitude of the vertical velocity never changes sign as corresponding to a first internal-wave mode.

Fig. 13 plots the simulated vertical sections for the disturbed variables from Eqs. (13)–(15). By comparing the simulated horizontal velocity plot (Fig. 13B) with the observed velocity sections in an early state of wave generation (Fig. 4B), it can be seen that the main observed behaviours are reproduced. Evidently, the solution can only approach this situation prior to the switching of the resonance process, which have just happened by the time of the section presented in Fig. 4C. With regard to the disturbances in vertical velocity, the simulated values, for an early state of the wave generation (Fig. 13C), match quite well with the observed values (Fig. 5) above the 150 m depth. Below this depth, the behaviour of the vertical velocity seems to be related to isopycnal disturbances resulting from a near-ground effect of the flow forcing over the bottom topography. However, the response from the near-ground layers behaves nearly as predicted.

5. Discussion

We have described the main physical characteristics of the high-amplitude steady waves established over Camarinal Sill during the maximum outflow phase of the tidal current during a neap tide. These waves are readily recognised by specially intense BWP produced at the surface.

The resonant processes causing the observed steady waves are activated under subcritical conditions over the sill ($G^2 = 0.73$). It has been observed from the analysis of other arrested-wave events (not included in the present study) that steady waves were not generated with internal Froude numbers outside the interval of 0.6–0.75. This may be caused by a departure of the wavelength of the steady vertical mode, corresponding to these hydraulic conditions, from the topographic wavelengths (Fig. 10). In this case, when $G^2 < 0.6$ and $G^2 > 0.75$, the resulting wavelengths are, respectively, smaller and larger than

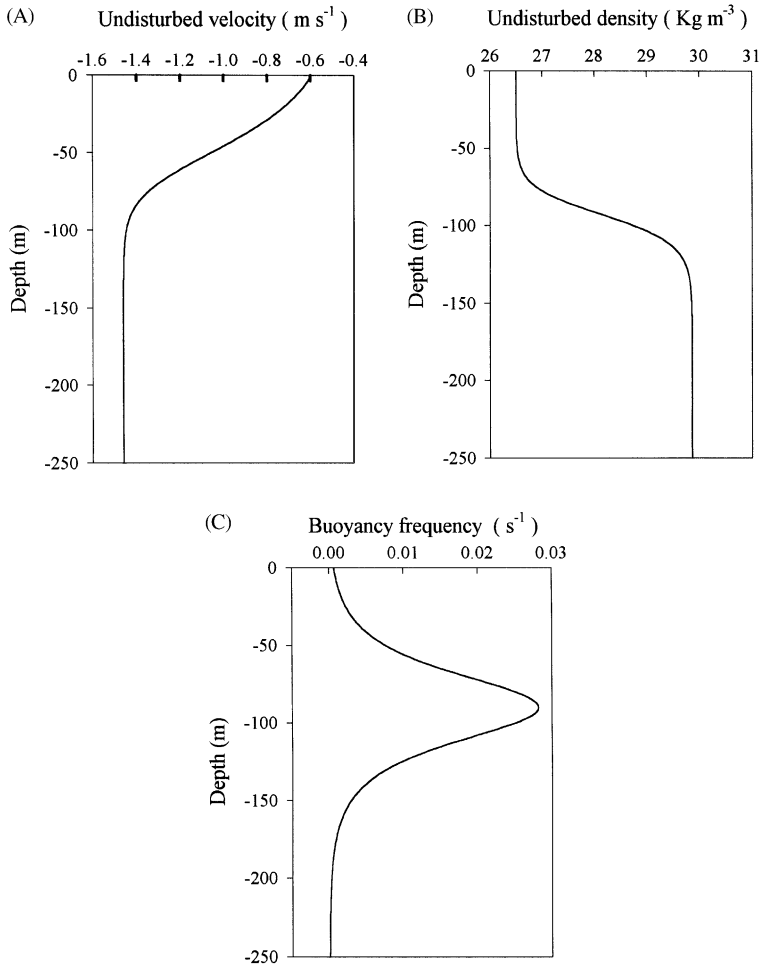

Fig. 11. Smoothed profiles characterising the conditions prior to the internal waves appearance. (A) Undisturbed velocity profile, $U(z)$; (B) undisturbed density profile, $\bar{\rho}(z)$; (C) buoyancy frequency, $N(z)$.

the resonant wavelength. Consequently, topographic resonant waves are not developed.

Since these internal wave events always occur under subcritical conditions, an internal bore is not possible. The internal bore, on the other hand, is formed when the flow is supercritical downstream of the sill. By this time, the flow is critical at the sill crest (Armi and Farmer, 1988). With critical conditions prevailing over the sill, it is clear that steady waves over the sill are not possible. Therefore, the internal bore and the resonant topographic waves are quite different phenomena.

Resonant topographic waves are expected during neap tides, when subcritical conditions exist, and therefore must be a characteristic of neap-tide periods. This would explain why these waves were not detected in the study of Armi and Farmer (1988), which was basically conducted during a spring-tide period. La Violette and Lacombe (1988) describe a structure (observed during neap tide) that is clearly identified with the resonant topographic waves discussed here. Richez (1994) found two different internal structures at Camarinal Sill, one in spring tide and the another in neap

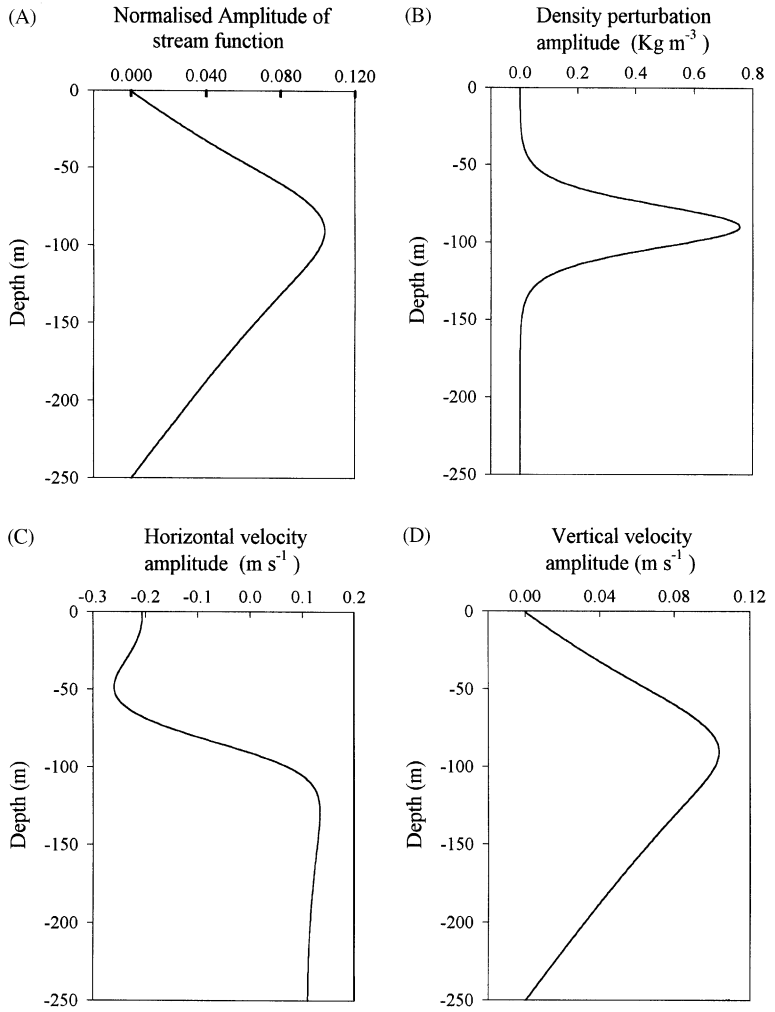

Fig. 12. Amplitudes of the steady mode disturbance for: (A) Stream Function (normalised eigenfunction); (B) density ; (C) horizontal velocity ; (D) vertical velocity.

tide. It could be that Richez's second structure is what we have identified and studied in this work.

To explain the physical origin of resonant topographic waves, we have use a linearised, two-dimensional, non-rotating, non-hydrostatic, horizontally unbounded fluid, assuming Boussinesq approximation and negligible dissipative effects. After a normal modal analysis, the so-called Taylor–Goldstein equation is obtained and solved numerically for resonant conditions ($c = 0$). The solution is a single oscillation mode with a wavelength of 1100 m, which is close to the main across-sill topographic wavelength. Such a mode efficiently reproduces the pattern of the observed variable fields associated with the wave at an initial state of generation when non-linear effects can be neglected. As a result, we conclude that the studied perturbation is a resonant wave, trapped by the flow, and produced by the interaction between the flow and the bottom topography of the sill.

The mixing processes induced by these waves can be particularly important in understanding the biological and geo-chemical cycles in the Strait of Gibraltar. This mixing is enabled by an enhancement of vertical shear created by the waves at the trough along with vertical advection. The shear

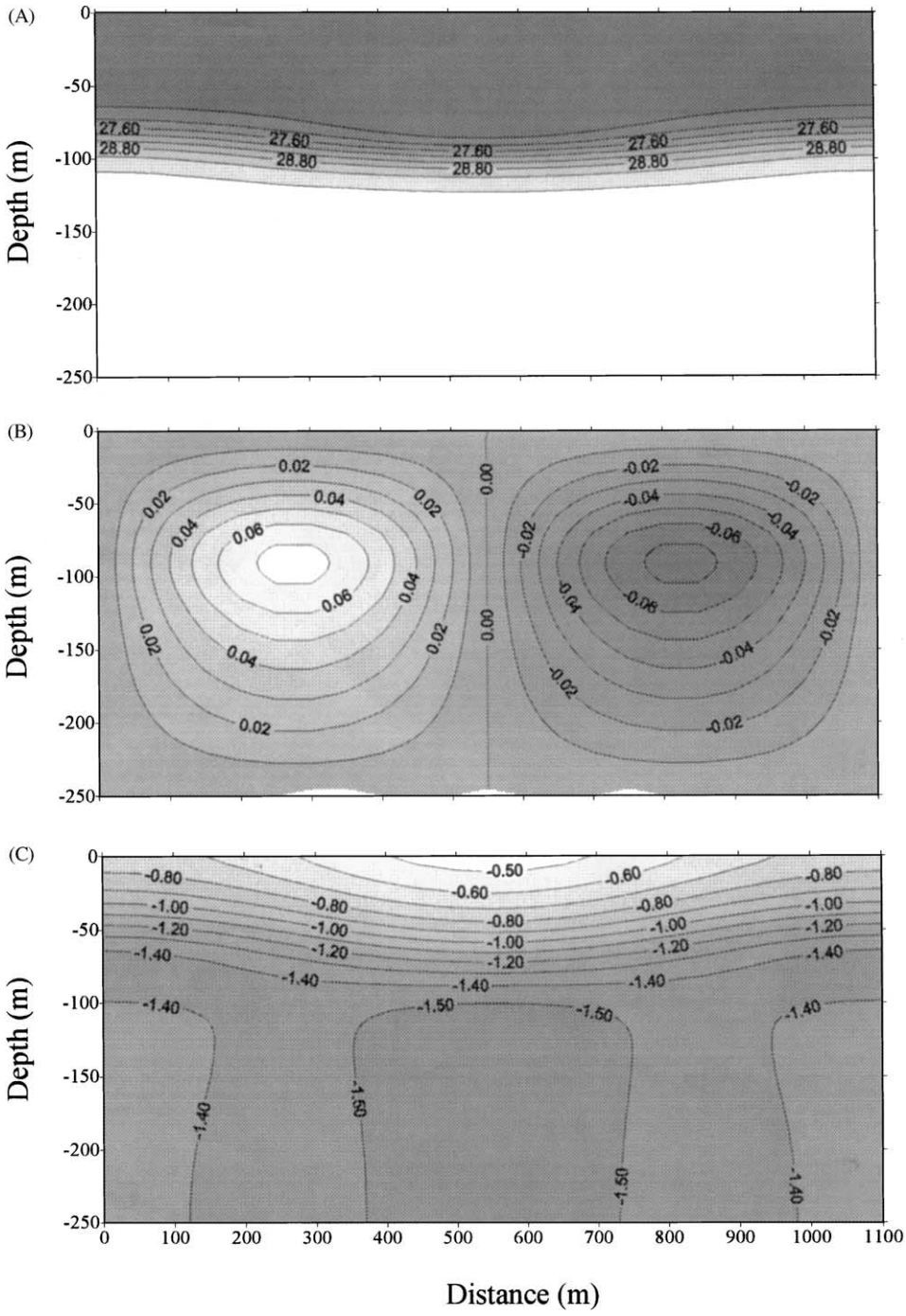

Fig. 13. Simulated vertical sections along a wave length ($\lambda = 1100$ m) of disturbed flow variables corresponding to the steady mode disturbance. (A) disturbed density profile in σ_t units; (B) disturbance of vertical velocity in m s^{-1}; (C) disturbed horizontal velocity in m s^{-1}.

and vertical advection combine to produce a suitable mechanism to carry the suspended matter upward into the upper layer.

Following Armi and Farmer (1988) and Wesson and Gregg (1994), the mixing processes at the Strait of Gibraltar are expected to be more intense during the internal bore. In this sense, the intensity of the mixing would decrease during neap tides or even within the spring-tide cycle during some moderate outflow intensity in which critical conditions are not achieved over the sill. During these periods, the resonant wave generation replaces the mixing mechanism, thus reducing the expected sharp decrease in mixing.

During our observation period (24–28 November 1998) we found that the resonant wave events exhibited a diurnal periodicity (Fig. 6), which provided a certain continuity of the mixing phenomena at Camarinal Sill. The reflector concentration in the whole of the water column also clearly increased (Fig. 8). After this event the increase seemed to be related to further mixing induced by arrested waves after their release and propagation toward the Mediterranean.

Acknowledgements

Authors thank SECEG for providing the means to carry out the survey, and the crew of the R.V. *Investigador* for a good assistance to our measurement program. This study was partially funded by the European project CANIGO (MAS3-Ct96-0060). Authors also thank the helpful comments of Dr. García Lafuente and LCDR Dave McDowel from US European Meteorology and Oceanography Center for his review of the English. Historical data about boiling-water events in the Strait of Gibraltar were kindly supplied by the Army Hydrographic Institute of Cádiz.

References

Armi, L., Farmer, D.M., 1988. The flow of Mediterranean water through the Strait of Gibraltar. Progress in Oceanography 21, 1–105.

Boyce, F.M., 1975. Internal waves in the Strait of Gibraltar. Deep-Sea Research 22, 597–610.

Brandt, P., Alpers, W., Backhaus, J.O., 1996. Study of the generation and propagation of internal waves in the Strait of Gibraltar using a numerical model and synthetic aperture radar images of the European ERS-a satellite. Journal of Geophysical Research 101, 14237–14252.

Bray, N.A., Winant, C.D., Kinder, T.H., Candela, J., 1990. Generation and kinematics of the internal tide in the Strait of Gibraltar. In: Pratt, L.J. (Ed.), The Physical Oceanography of Sea strait. Kluwer Academic Publishers, Dordrecht, pp. 477–491.

Bruno, M., Mañanes, R., Alonso, J.J., Izquierdo, A., Tejedor, L., Kagan, B., 2000. Vertical structure of the semidiurnal tidal currents at Camarinal Sill, the strait of Gibraltar. Oceanol. Acta 23 (1), 15–24.

Cavanie, A.G., 1972. Observations de fronts internes dans le detroit de Gibraltar pendant la Campagne Océanographique OTAN 1970 et interpretation des résultats par un modéle mathématique. Mémoires de la Societe des Sciences de Liége 6, 27–41.

Echevarría, F., García Lafuente, J., Bruno, M., Gorsky, G., Goutx, M., González, N., García, C.M., Gómez, F., Vargas, J.M., Picheral, M., Striby, L., Varela, M., Alonso, J.J., Reul, A., Cózar, A., Prieto, L., Sarhan, T., Plaza, F., Jiménez-Gómez, F., 2002. Physical-biological coupling in the Strait of Gibraltar. Deep-Sea Research II 49 (19), 4115–4130.

Farmer, D., Armi, L., 1999. The generation and trapping of solitary waves over topography. Science 283, 188–190.

Frasseto, R., 1964. Short period vertical displacements of the upper layers in the Strait of Gibraltar. Technical Report 30, SACLANT ASW Rsearch Centre, La Spezia, Italy, 49 pp.

Izquierdo, A., Tejedor, L., Sein, D.V., Bachaus, J.O., Brandt, P., Rubino, A., Kagan, B.A., 2001. Control variability and internal bore evolution in the Strait of Gibraltar: A 2D two-layer model study. Estuarine, Coastal and shelf Science 53, 637–651.

Kundu, P.K., 1990. Fluid Mechanics. Academic Press, New York, 658 pp.

La Violette, P.E., Kinder, T.H., Green, D.W., 1986. Measurement of internal waves in the Strait of Gibraltar using a shore-based radar. Technical Report 118, Naval Ocean Research and Development Activity, National Space Technology Laboratory, Bay of St. Louis, Miss, 13 pp.

La Violette, P.E., Lacombe, H., 1988. Tidal-induced pulses in the flow through the Strait of Gibraltar. Oceanology Acta, SP, 13–17.

New, A.L., Pingree, R.D., 1992. Local generation of internal soliton packets in the central Bay of Biscay. Deep-Sea Research 39, 1521–1534.

Purdy, J., 1840. The new sailing directory for the Strait of Gibraltar and the western division of the Mediterranean Sea.

Richez, C., 1994. Airbone synthetic aperture radar tracking of internal waves in the Strait of Gibraltar. Progress in Oceanography 33, 93–159.

Ruiz-Cañavate, A., Rico, J., 1996. Hourly oceanographic and acoustic variations in the Strait of Gibraltar, and multibeam echosounder technology. International Hydrographic Review LXXIII (2), 109–119.

Tofiño, V., 1832. Derrotero de las costas de España en el Mediterráneo y su correspondiente de África, Dirección de Hidrografía.

Watson, G., Robinson, I.S., 1990. A study of internal wave propagation in the Strait of Gibraltar using shore-based radar images. Journal of Physical Oceanography 20, 374–395.

Wesson, J.C., Gregg, M.C., 1994. Mixing ant Camarinal Sill in the Strait of Gibraltar. Journal of Physical Oceanography 21, 185–204.

Ziegenbein, J., 1969. Short internal waves in the Strait of Gibraltar. Deep-Sea Research 16, 479–487.